Hybrid Electromagnetic Nanomaterials Based on Polydiphenylamine-2-carboxylic Acid

Sveta Zhiraslanovna Ozkan [1,*], **Aleksandr Ivanovich Kostev** [1], **Galina Petrovna Karpacheva** [1],
Petr Aleksandrovich Chernavskii [1,2], **Andrey Aleksandrovich Vasilev** [1] **and**
Dmitriy Gennad'evich Muratov [1]

[1] A.V. Topchiev Institute of Petrochemical Synthesis, Russian Academy of Sciences, 29 Leninsky Prospect,
119991 Moscow, Russia; kostev@ips.ac.ru (A.I.K.); gpk@ips.ac.ru (G.P.K.); chern5@inbox.ru (P.A.C.);
vasilev@ips.ac.ru (A.A.V.); muratov@ips.ac.ru (D.G.M.)
[2] Department of Chemistry Lomonosov Moscow State University, 1-3 Leninskie Gory, 119991 Moscow, Russia
[*] Correspondence: ozkan@ips.ac.ru

check for updates

Abstract: Hybrid ternary nanomaterials based on conjugated polymer polydiphenylamine-2-carboxylic acid (PDPAC) (poly-*N*-phenylanthranilic acid), Fe_3O_4 nanoparticles and single-walled carbon nanotubes (SWCNT) were prepared for the first time. Polymer–metal–carbon Fe_3O_4/SWCNT/PDPAC nanocomposites were synthesized via in situ oxidative polymerization of diphenylamine-2-carboxylic acid (DPAC) by two different ways: in an acidic medium and in the interfacial process in an alkaline medium. In an alkaline medium (pH 11.4), the entire process of Fe_3O_4/SWCNT/PDPAC-1 synthesis was carried out in one reaction vessel without intermediate stages of product extraction and purification. In an acidic medium (pH 0.3), to prepare the Fe_3O_4/SWCNT/PDPAC-2 nanocomposites, prefabricated magnetite nanoparticles were deposited on the surface of obtained SWCNT/PDPAC-2. The phase composition of the nanocomposites does not depend on the synthesis reaction medium pH. The influence of the reaction medium pH on the structure, morphology, thermal, magnetic, and electrical properties of the obtained ternary nanocomposites was studied.

Keywords: polydiphenylamine-2-carboxylic acid; conjugated polymers; polymer–metal–carbon nanocomposites; in situ oxidative polymerization; single-walled carbon nanotubes; Fe_3O_4 nanoparticles; magnetic fluids; electromagnetic nanomaterials

1. Introduction

Modern technology demands the creation of new generation materials with a range of required properties. In recent decades, polymer nanocomposites have become a prominent area of current research promoted by rapid developments in both polymer science and nanotechnology [1–6]. Polymer nanocomposites have unique physicochemical properties owing to synergistic performance derived from each component. Such materials are of growing interest to researchers due to their great potentials for a wide range of applications [7–16]. Polymer–metal–carbon nanocomposites containing conjugated polymers, magnetic nanoparticles and carbon nanomaterials take a special place in this class of polymer nanocomposites [17,18]. Such ternary nanocomposites are superparamagnetic [19–22] and can effectively absorb electromagnetic radiation [20–27]. Due to the combination of their electrical and magnetic properties, these electromagnetic nanocomposites can be used for medical applications (immobilization of trypsin in a nanocomposite for protein digestion) [28]; to produce sensors [29]; supercapacitors [30–32]; as cathode materials for rechargeable batteries and fuel cells [33–35]; and as anticorrosive coatings [36].

Polyaniline, polypyrrole, polythiophene, and their derivatives are examples of conjugated polymers used to synthesize ternary nanocomposites. Graphene [30–32], reduced graphene oxide (RGO) [25,27,29,30,36,37], and carbon nanotubes (CNT) [19,21,26,35,38–40] can be used as carbonaceous nanofillers. The choice of carbon nanomaterials is explained by their excellent structural and functional properties [41,42]. Ternary nanocomposites use Fe_3O_4 [19,21,26,27,36,38–40], Co_3O_4 [25,30,32], Fe_2O_3 [29,37], FeCoO [35], and $CoFe_2O_4$ [31] as magnetic nanoparticles.

There are two most common approaches to the preparation of polymer–metal–carbon nanocomposites. The first way is the in situ oxidative polymerization of aromatic amines in the presence of magnetic nanoparticles immobilized on the surface of carbon nanomaterials [19,20,23,29,39,40]. The second approach provides the in situ oxidative polymerization of aromatic amines in the presence of carbon nanomaterials followed by the deposition of magnetic nanoparticles on the polymer surface [21,22,25,38]. Depending on the synthesis way, prefabricated magnetite nanoparticles uniform in size and shape were used to synthesize the Fe_3O_4/MWCNT and Fe_3O_4/RGO nanocomposites [19,20,23]. Graphene oxide was reduced with hydrazine [20,22,25]. Multi-walled carbon nanotubes (MWCNT) were pretreated with concentrated acids to functionalize their surface [21,23]. Modified Fe_3O_4 nanoparticles were added to the reaction solution containing MWCNT/PANI [21].

Earlier, we obtained hybrid nanomaterials based on poly-3-amine-7-methylamine-2-methylphenazine (PAMMP), single-walled carbon nanotubes (SWCNT), and Fe_3O_4 nanoparticles via in situ chemical oxidative polymerization of 3-amine-7-methylamine-2-methylphenazine hydrochloride (Neutral Red) in the presence of prefabricated Fe_3O_4/SWCNT nanocomposites [43]. The Fe_3O_4/SWCNT/PAMMP nanomaterials are superparamagnetic.

In the present study, ternary nanocomposites based on polydiphenylamine-2-carboxylic acid (PDPAC), Fe_3O_4 nanoparticles, and SWCNT were prepared for the first time. The Fe_3O_4/SWCNT/PDPAC nanomaterials were synthesized under different conditions of oxidative polymerization: in the interfacial process in an alkaline medium (pH 11.4) and in a 5 M solution of sulfuric acid (pH 0.3). A comparative analysis of the structure, morphology, thermal, magnetic, and electrical properties depending on the synthesis conditions was done.

2. Experimental

2.1. Materials

Diphenylamine-2-carboxylic acid (*N*-phenylanthranilic acid) ($C_{13}H_{11}O_2N$) (analytical grade), sulfuric acid (reagent grade), aqueous ammonia (reagent grade), and chloroform (reagent grade), as well as iron (II) sulfate (high-purity grade) and iron (III) chloride (high-purity grade) were used as received. Ammonium persulfate (analytical grade) was purified by recrystallization from distilled water. The aqueous solutions of reagents were prepared with the use of distilled water. SWCNT from Carbon Chg, Ltd. (Moscow, Russia) were produced using the electric arc discharge technique with a Ni/Y catalyst (d = 1.4–1.6 nm, l = 0.5–1.5 μm).

2.2. Synthesis of Fe_3O_4/SWCNT

The synthesis of Fe_3O_4 nanoparticles immobilized on the SWCNT surface was carried out via hydrolysis of iron (II) and (III) salts mixture with a molar ratio of 1:2 in a solution of ammonium hydroxide in the presence of SWCNT at 60 °C. For that, 0.86 g of $FeSO_4 \cdot 7H_2O$ and 2.35 g of $FeCl_3 \cdot 6H_2O$ were dissolved in 20 mL of distilled water (Table 1). 0.03 g of SWCNT were added to the resulting solution and heated to 60 °C, then 5 mL of ammonium hydroxide NH_4OH were added. The resulting suspension was heated on a steam bath to 80 °C and stirred for 0.5 h. The suspension was cooled at ambient temperature under intensive stirring for 1 h. The obtained Fe_3O_4/SWCNT nanocomposite was filtered off, washed with distilled water until neutral reaction of the filtrate, and vacuum-dried over KOH to constant weight.

Table 1. Conditions for synthesis of Fe_3O_4/SWCNT and Fe_3O_4/SWCNT/PDPAC nanocomposites.

Nanomaterials Abbreviations	Fe, % *	Preparation Method	** Amount of SWCNT, g	Amount of DPAC, g	*** Amount of Iron Salts, g	
					Fe (II)	Fe (III)
$F_{34}C_3$ ****	61.2	Synthesis of Fe_3O_4/SWCNT in an alkaline medium	0.03	0	0.86	2.35
$F_{34}C_3$P-1	33.5	Polymerization of DPAC in the interfacial process in an alkaline medium with Fe_3O_4/SWCNT	0.03	1.0	0.86	2.35
$F_{18}C_3$P-1	17.9				0.43	1.18
$F_{14}C_3$P-1	12.0				0.22	0.59
F_7C_3P-1	6.4				0.11	0.29
F_7C_{10}P-1	8.4		0.1		0.11	0.29
$F_{34}C_3$P-2	34.7	Precipitation of Fe_3O_4 onto the surface of the SWCNT/PDPAC, prepared in an acidic medium	0.019	0.64	0.43	1.18
$F_{18}C_3$P-2	17.8				0.27	0.73
$F_{14}C_3$P-2	13.4				0.11	0.29
F_7C_3P-2	7.6				0.054	0.15
F_7C_{10}P-2	6.2		0.064		0.054	0.15

* According to ICP-AES data. ** C_{SWCNT} = 3 and 10 wt. % relative to the monomer weight. *** $FeSO_4 \cdot 7H_2O$ and $FeCl_3 \cdot 6H_2O$. **** Fe_3O_4/SWCNT.

2.3. Preparation of Fe₃O₄/SWCNT/PDPAC Nanocomposites

2.3.1. Preparation of Fe₃O₄/SWCNT/PDPAC Nanocomposites in the Interfacial Process in an Alkaline Medium

The following method was used to prepare the Fe_3O_4/SWCNT/PDPAC nanocomposite in the interfacial process in an alkaline medium. First, the synthesis of Fe_3O_4 nanoparticles of the required concentration, immobilized on the surface of SWCNT, was carried out as described in 2.2 at 55 °C. The amount of carbon nanotubes is C_{SWCNT} = 3 and 10 wt. % relative to the monomer weight. Diphenylamine-2-carboxylic acid (DPAC) solution with the required concentration (0.15 mol/L, 1 g) in a mixture of an organic solvent—chloroform (60 mL) and NH_4OH (5 mL)—was added to the obtained aqueous alkaline suspension of the Fe_3O_4/SWCNT nanocomposite. The process was conducted at 55 °C with continuous intensive stirring for 0.5 h. The suspension was cooled at room temperature with vigorous stirring for 1 h. After that, the suspension was thermostated under continuous stirring at 0 °C, and the aqueous solution of ammonium persulfate (0.3 mol/L, 1.96 g) was added. The solutions of the organic and aqueous phases were mixed in one shot without gradual dosing of the reagents. The volume ratio of organic and aqueous phases was 1:1 (V_{total} = 120 mL). The polymerization reaction continued for 3 h under intensive stirring at 0 °C. When the synthesis was completed, the reaction mixture was precipitated in a threefold excess of 1 M H_2SO_4. The obtained product was filtered off and washed repeatedly with distilled water until neutral reaction of the filtrate. Since the product was in a neutral basic form, it was vacuum dried over alkali (KOH) to constant weight. The yield was 1.058 g for the nanocomposite prepared at $C_{FeSO4·7H2O}$ = 0.86 g and $C_{FeCl3·6H2O}$ = 2.35 g, C_{SWCNT} = 0.03 g (3 wt. % relative to the monomer weight).

Nanocomposites based on PDPAC, SWCNT, and magnetite nanoparticles obtained in an alkaline medium were marked as Fe_3O_4/SWCNT/PDPAC-1. PDPAC was synthesized under the same conditions [44] to compare the structure and properties of nanocomposites and polymer, and marked as PDPAC-1.

The Fe_3O_4/SWCNT/PDPAC-1 nanocomposites depending on synthesis conditions in alkaline medium were marked as F_xC_yP-*1*, where *F*—Fe_3O_4, *C*—SWCNT, *P*—PDPAC, *x*—the iron content according to ICP-AES data, and *y*—the SWCNT content relative to the monomer weight (Table 1).

2.3.2. Preparation of Fe₃O₄/SWCNT/PDPAC Nanocomposites in an Acid Medium

The following method was used to prepare the Fe_3O_4/SWCNT/PDPAC nanocomposite in an acidic medium. First, the SWCNT/PDPAC nanocomposite was synthesized. For that, SWCNT were added to the solution of DPAC (0.1 mol/L, 0.64 g) in 5 M H_2SO_4 and stirred in an ultrasonic bath at room temperature for 0.5 h. The mixture was heated to 25 °C. The amount of carbon nanotubes was C_{SWCNT} = 3 and 10 wt. % relative to the monomer weight. Then, for the oxidative polymerization of DPAC in the presence of SWCNT, an aqueous solution of ammonium persulfate (0.2 mol/L, 1.368 g) in the same solvent (1/4 of total volume, V_{total} = 30 mL) was added dropwise to the suspension previously thermostated at 0 °C under continuous stirring. The synthesis was carried out during 3 h under intensive stirring at 0 °C. When the reaction was completed, the mixture was precipitated in 200 mL of distilled water. The obtained SWCNT/PDPAC nanocomposite was filtered off and washed repeatedly with distilled water until there was neutral reaction of the filtrate. The synthesis of Fe_3O_4 nanoparticles was carried out by a known method via hydrolysis of iron (II) and (III) salts mixture in a solution of ammonium hydroxide [45]. To synthesize Fe_3O_4 nanoparticles of the required concentration, $FeSO_4·7H_2O$ and $FeCl_3·6H_2O$ with a molar ratio of 1:2 were dissolved in 20 mL of distilled water and heated to 60 °C, then 5 mL of ammonium hydroxide NH_4OH were added. The reaction mixture was heated on a steam bath to 80 °C and stirred for 0.5 h. Freshly prepared SWCNT/PDPAC nanocomposite was added immediately, without preliminary drying, to the obtained Fe_3O_4 suspension. The reaction mixture was stirred in an ultrasonic bath at ambient temperature for 0.5 h; then, to remove the liquid phase, it was heated to 60 °C in a crystallizing pan until precipitation. The obtained product was

filtered off, washed repeatedly with distilled water to an uncolored filtrate, and to avoid dedoping, vacuum dried over $CaCl_2$ to constant weight. The yield was 0.82 g for the nanocomposite prepared at $C_{FeSO_4 \cdot 7H2O}$ = 0.43 g and $C_{FeCl3 \cdot 6H2O}$ = 1.175 g, with C_{SWCNT} = 0.019 g (3 wt. % relative to the monomer weight).

Nanocomposites based on PDPAC, SWCNT, and magnetite nanoparticles obtained in an acidic medium were marked as Fe_3O_4/SWCNT/PDPAC-2. To compare the structure and properties of nanocomposites and polymer, PDPAC was synthesized under the same conditions [46,47] and marked as PDPAC-2.

The Fe_3O_4/SWCNT/PDPAC-2 nanocomposites depending on synthesis conditions in acidic medium were marked as F_xC_yP-2, where F—Fe_3O_4, C—SWCNT, P—PDPAC, x—the iron content according to ICP-AES data, and y—the SWCNT content relative to the monomer weight (Table 1).

2.4. Preparation of Suspensions for Magnetic Fluids

The suspensions of the Fe_3O_4/SWCNT and Fe_3O_4/SWCNT/PDPAC nanocomposites in ethanol were prepared. For this, 0.01 g of the nanocomposite was added to 5 mL of ethanol, mixed thoroughly, and left in a closed vessel to prevent evaporation of the solvent.

2.5. Characterization

The molecular mass of diphenylamine-2-carboxylic acid polymers was measured by GPC using Water's 150C chromatograph (San Diego, CA, USA) equipped with PLgel 5 μm MIXED-C GPC columns (Santa Clara, CA, USA), using N-methylpyrrolidone as an eluent at 60 °C. The eluent flow rate was 1 mL/min. Volume of the injected sample was 150 mL. Calibration was performed on polystyrene. RI-detector was used. Accuracy of MM definition is ~5%.

The metal content in the nanocomposites was measured quantitatively by an inductively coupled plasma atomic emission spectroscopy method (ICP-AES) using a Shimadzu ICP emission spectrometer (ICPE-9000).

FTIR spectra were measured in air on a Bruker IFS 66v FTIR spectrometer (Karlsruhe, Germany) in the range of 400–4000 cm^{-1} and analyzed with Soft-Spectra software. The samples were prepared as KBr pressed pellets. Attenuated total reflection (ATR) FTIR spectra of the samples in the attenuated total reflectance mode were recorded using a HYPERION-2000 IR microscope (Bruker, Karlsruhe, Germany) coupled with the Bruker IFS 66v FTIR spectrometer in the range of 600–4000 cm^{-1} (150 scans, ZnSe crystal, resolution of 2 cm^{-1}).

An X-ray diffraction study was performed in ambient atmosphere using a Difray-401 X-ray diffractometer (Scientific Instruments Joint Stock Company, Saint-Petersburg, Russia) with Bragg–Brentano focusing on CrK_α radiation, λ = 0.229 nm. The results of X-ray diffraction analysis were used to calculate the size distribution of the coherent scattering regions of crystallites [48] in magnetic nanoparticles.

An electron microscopic study was performed using a LEO912 AB OMEGA transmission electron microscope (Bioz Inc., Los Altos, CA, USA) and a Hitachi TM 3030 scanning electron microscope (Hitachi High-Technologies Corporation, Fukuoka, Japan) with magnification up to 30,000 and 30 nm resolution. The size of nanoparticles is determined using the EsiVision software (eVision Software, The Hague, The Netherlands).

A vibration magnetometer was used to study the magnetic characteristics of the systems. The cell of the vibration magnetometer was designed as a flow quartz microreactor, which made it possible to study chemical transformations in the in situ mode [49]. Specific magnetization depending on the magnetic field value was measured; magnetic characteristics of the samples at room temperature were determined.

The AC conductivity was measured with a 6367A precision LCR-meter (Microtest Co., Ltd., New Taipei City, Taiwan) in the frequency range of 0.1 Hz–1.0 MHz.

Thermogravimetric analysis (TGA) was performed on a Mettler Toledo TGA/DSC1 (Giessen, Germany) in the dynamic mode in the range of 30–1000 °C in air and in the argon flow. The weight of the samples was 100 mg, the heating rate was 10 °C/min, and the argon flow velocity was 10 mL/min. Calcined aluminum oxide was used as a reference. The samples were analyzed in an Al_2O_3 crucible.

Differential scanning calorimetry (DSC) was performed on a Mettler Toledo DSC823^e calorimeter (Giessen, Germany). The samples were heated at the rate of 10 °C/min in the nitrogen atmosphere, with the nitrogen flow rate of 70 mL/min. The measurement results were processed with the service program STARe supplied with the device.

3. Results and Discussion

3.1. Synthesis and Characterization of Nanomaterials

Synthesis methods were developed to prepare polymer–metal–carbon nanocomposites based on polydiphenylamine-2-carboxylic acid (PDPAC) first synthesized by the authors [44,46], single-walled carbon nanotubes (SWCNT), and magnetite nanoparticles (Fe_3O_4). Hybrid Fe_3O_4/SWCNT/PDPAC nanomaterials were synthesized via in situ oxidative polymerization of diphenylamine-2-carboxylic acid (DPAC) in an acidic medium and in the interfacial process in an alkaline medium. Table 1 presents the conditions for synthesis of the nanocomposites. For comparison, polymers of diphenylamine-2-carboxylic acid were synthesized under the same conditions: in a NH_4OH solution in the presence of chloroform (PDPAC-1) and in 5 M H_2SO_4 (PDPAC-2). According to the GPC, the molecular mass of PDPAC-1 reached $M_w = 2.6 \times 10^4$, the degree of polymerization was more than 120, and the polydispersity index was 2.2 [44]. The PDPAC-2 molecular mass achieved $M_w = 1.1 \times 10^4$, the polymerization degree was above 50, and the index of polydispersity was 2.0 [46]. The oxidative polymerization in the heterophase system in the presence of chloroform reduces the probability of oxidative hydrolysis and macromolecules destruction owing to separation of reaction products and the oxidizer. This makes it possible to increase the molecular mass of PDPAC-1 by a factor of nearly 2.5 as compared to the homogeneous process.

Figure 1 shows the sequence of synthesis steps of the ternary nanomaterials.

In an alkaline medium (pH 11.4), the entire process of Fe_3O_4/SWCNT/PDPAC-1 synthesis was carried out in one reaction vessel without intermediate stages of disengagement and purification. The synthesis of Fe_3O_4 nanoparticles; their immobilization on the surface of SWCNT with the formation of Fe_3O_4/SWCNT nanocomposite; the anchorage of a monomer to Fe_3O_4/SWCNT by adding a DPAC solution in a mixture of chloroform and NH_4OH; and in situ interfacial oxidative polymerization in the presence of ammonium persulfate were performed stepwise (Figure 1a).

In an acidic medium (pH 0.3), to prepare the Fe_3O_4/SWCNT/PDPAC-2 nanocomposites, the in situ oxidative polymerization of DPAC in the presence of SWCNT was performed followed by the deposition of prefabricated magnetite nanoparticles on the surface of obtained SWCNT/PDPAC-2 (Figure 1b).

The formation of Fe_3O_4/SWCNT/PDPAC nanocomposite materials was confirmed by X-ray diffraction (XRD), FTIR spectroscopy, transmission electron microscopy (TEM), and scanning electron microscopy (SEM).
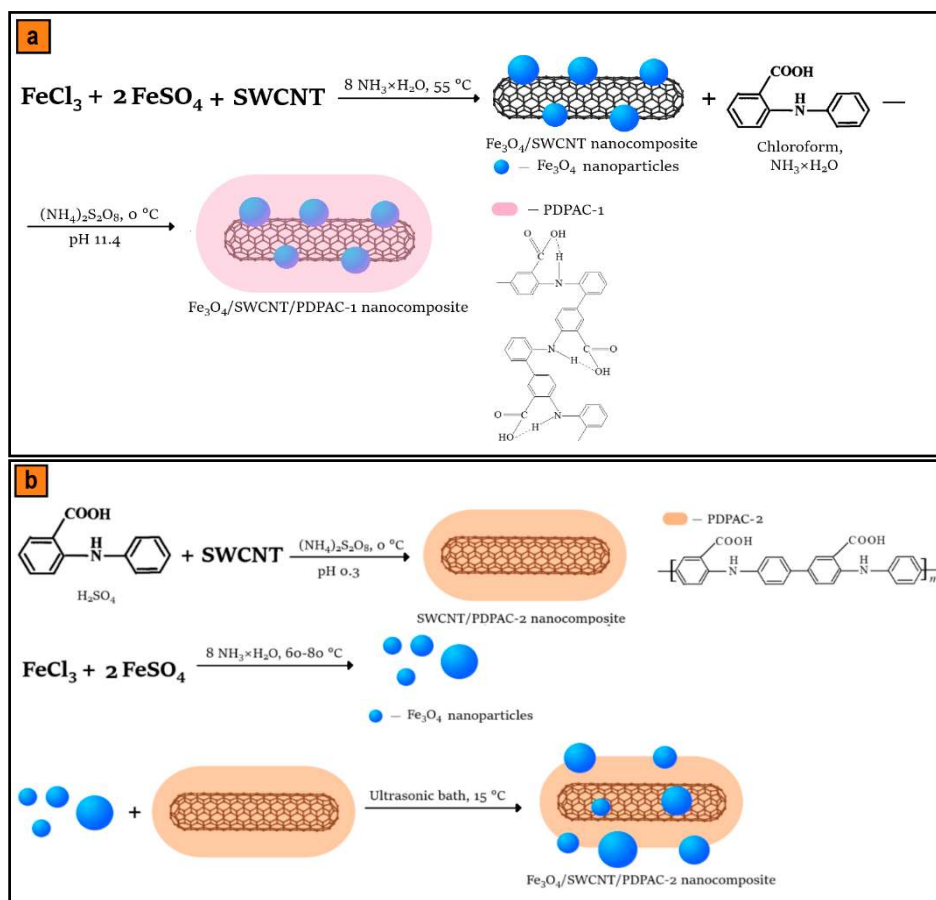
Figure 1. Synthesis sequence of Fe_3O_4/SWCNT/PDPAC in alkaline (**a**) and acidic media (**b**).

The data presented in Figure 2 allow us to conclude that the phase composition of the nanocomposites does not depend on the synthesis reaction medium pH. According to the XRD data, irrespective of the synthesis method, diffractograms of Fe_3O_4/SWCNT/PDPAC identify reflection peaks of Fe_3O_4 in the range of scattering angles $2\theta = 46.1°, 54.3°, 66.8°, 84.8°, 91.2°,$ and $102.2°$ (CrK_α radiation) [43]. These diffraction peaks correlate to Miller indices (220), (311), (400), (422), (511), and (440), respectively, and refer to the cubic structure of Fe_3O_4 (JCPDS 19-0629) [50]. As can be seen in Figure 3, electron diffraction confirms the crystalline nature and phase composition of Fe_3O_4 nanoparticles. The diffraction rings correspond to Fe_3O_4 crystals. Since the single plane of SWCNT does not give a diffraction pattern, there is no carbon phase reflection peak at $2\theta = 39.8°$. An amorphous halo in the range of scattering angles $2\theta = 20°–43°$ in the diffraction patterns of nanocomposites characterizes the polymer component (Figure 2b). The small wide diffraction peaks in the range of $2\theta = 20°–43°$ characterize the crystalline DPAC oligomers contained in the polymer fraction of nanomaterials obtained in the acidic medium (Figure 2c), which is also confirmed by the DSC data. Removal of the crystalline low molecular weight fraction by washing nanocomposites with acetone can lead to a dedoping of the polymer component.
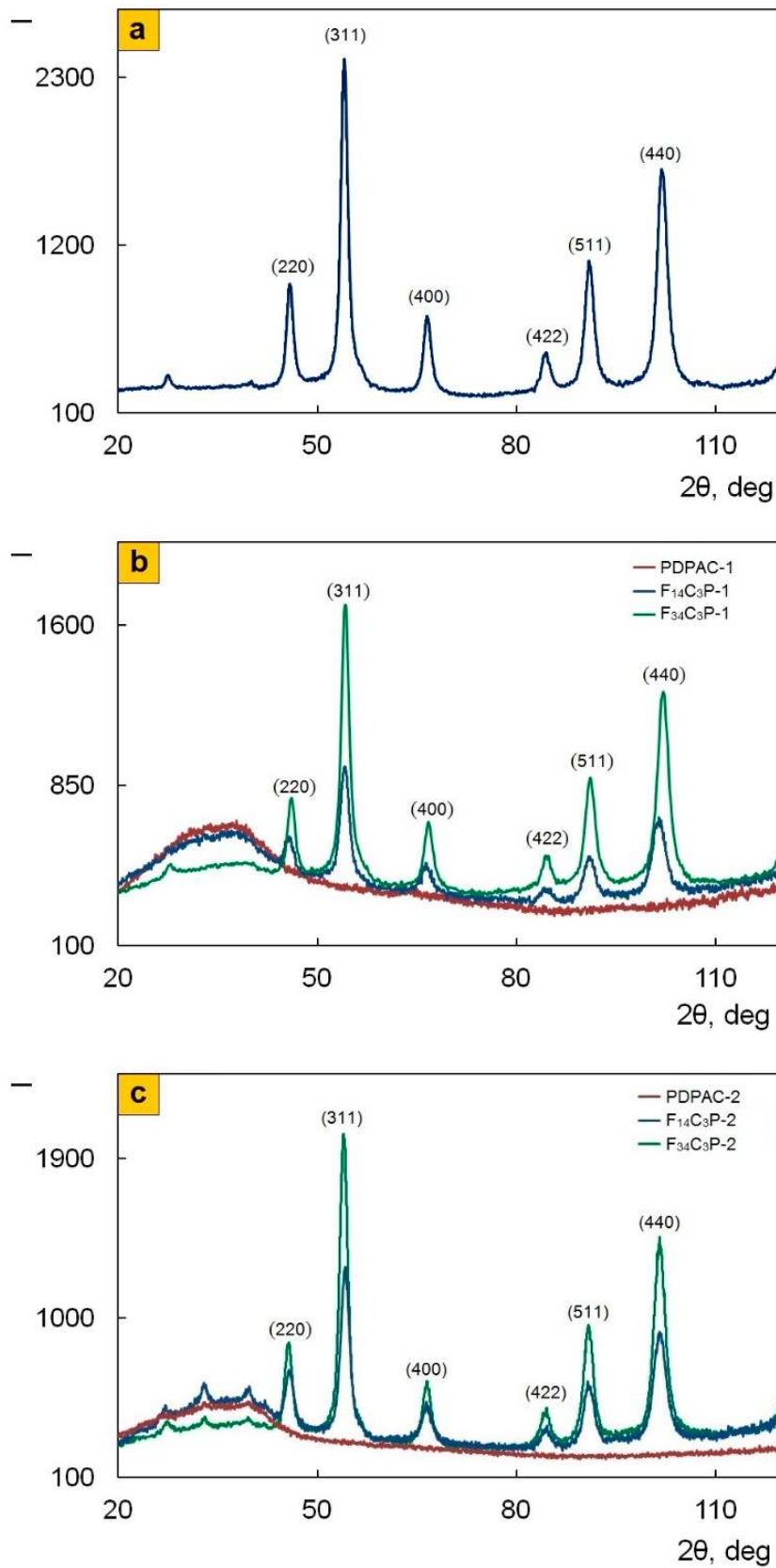
Figure 2. X-ray diffractograms of Fe_3O_4/SWCNT (**a**), PDPAC, and Fe_3O_4/SWCNT/PDPAC, prepared in alkaline (**b**) and acidic media (**c**).
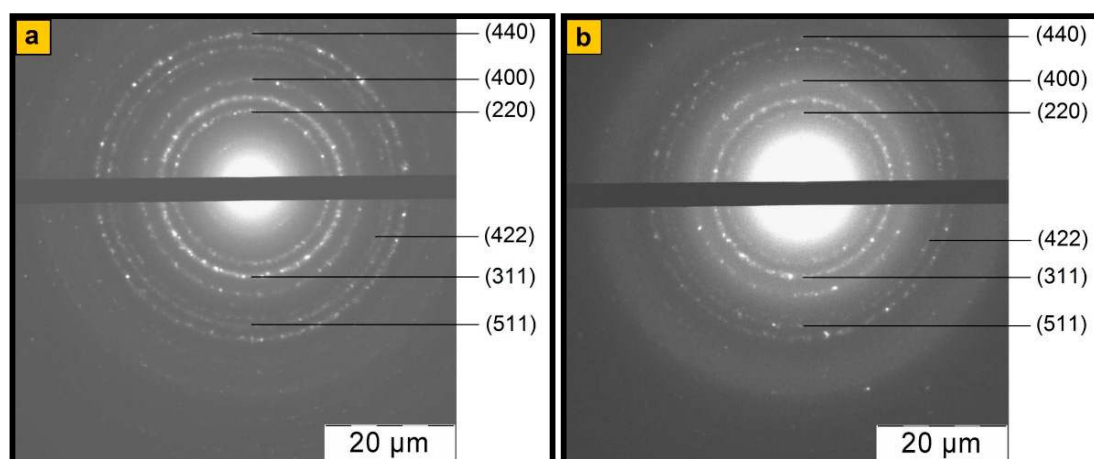
Figure 3. Fe_3O_4 diffraction images of Fe_3O_4/SWCNT/PDPAC, prepared in alkaline (**a**) and acidic media (**b**).

Table 2 demonstrates the volume fraction of materials. The fraction of amorphous and crystalline phases was calculated from the ratio of the areas of reflection peaks of the corresponding phases using standard samples. This technique is described in detail in [51]. As can be seen, the volume fraction of the crystalline low molecular weight fraction is negligible. Volume fraction of Fe_3O_4 in the nanocomposites reaches 62–95%.

Table 2. Volume fraction of materials.

Materials	Volume Fraction, %		
	Amorphous Polymer	Crystalline Polymer	Fe_3O_4
PDPAC-1	100.00	-	-
$F_{14}C_3P$-1	37.69	-	62.31
$F_{34}C_3P$-1	5.24	-	94.76
$F_{34}C_3$ *	-	-	100.00
PDPAC-2	95.60	4.40	-
$F_{14}C_3P$-2	28.99	2.35	68.66
$F_{34}C_3P$-2	6.21	0.75	93.05

* Fe_3O_4/SWCNT.

We have previously shown that, during the hydrolysis of iron (II) and (III) salts mixture in the solution of ammonium hydroxide in the presence of SWCNT, the synthesis of Fe_3O_4 nanoparticles and their immobilization on the surface of SWCNT with the formation of the metal–carbon Fe_3O_4/SWCNT nanocomposite occur simultaneously [43]. The XRD, TEM, and SEM data confirm the formation of Fe_3O_4/SWCNT (Figure 2a, Figure 4a, and Figure 5a). According to the FTIR data, during the Fe_3O_4/SWCNT/PDPAC-1 synthesis in the interfacial process in an alkaline medium, the polymer interacts with the Fe_3O_4/SWCNT surface by binding the carboxylate ion and iron to form the Fe–OOC bond. The FTIR spectra of Fe_3O_4/SWCNT/PDPAC-1 nanomaterials (Figure 6a) show a hypsochromic shift of the absorption band at 561 to 578 cm^{-1}, which corresponds to stretching vibrations of the $\nu_{Fe–O}$ bond. The intensity of this band grows with the increase of Fe_3O_4 in the Fe_3O_4/SWCNT/PDPAC-1 nanocomposites. There is also a long-wavelength shift in the absorption band of the stretching vibrations of $\nu_{C=O}$ bonds in the carboxyl group to 1672 cm^{-1} compared to the location of this band in the polymer at 1682 cm^{-1} (Figure 7a).
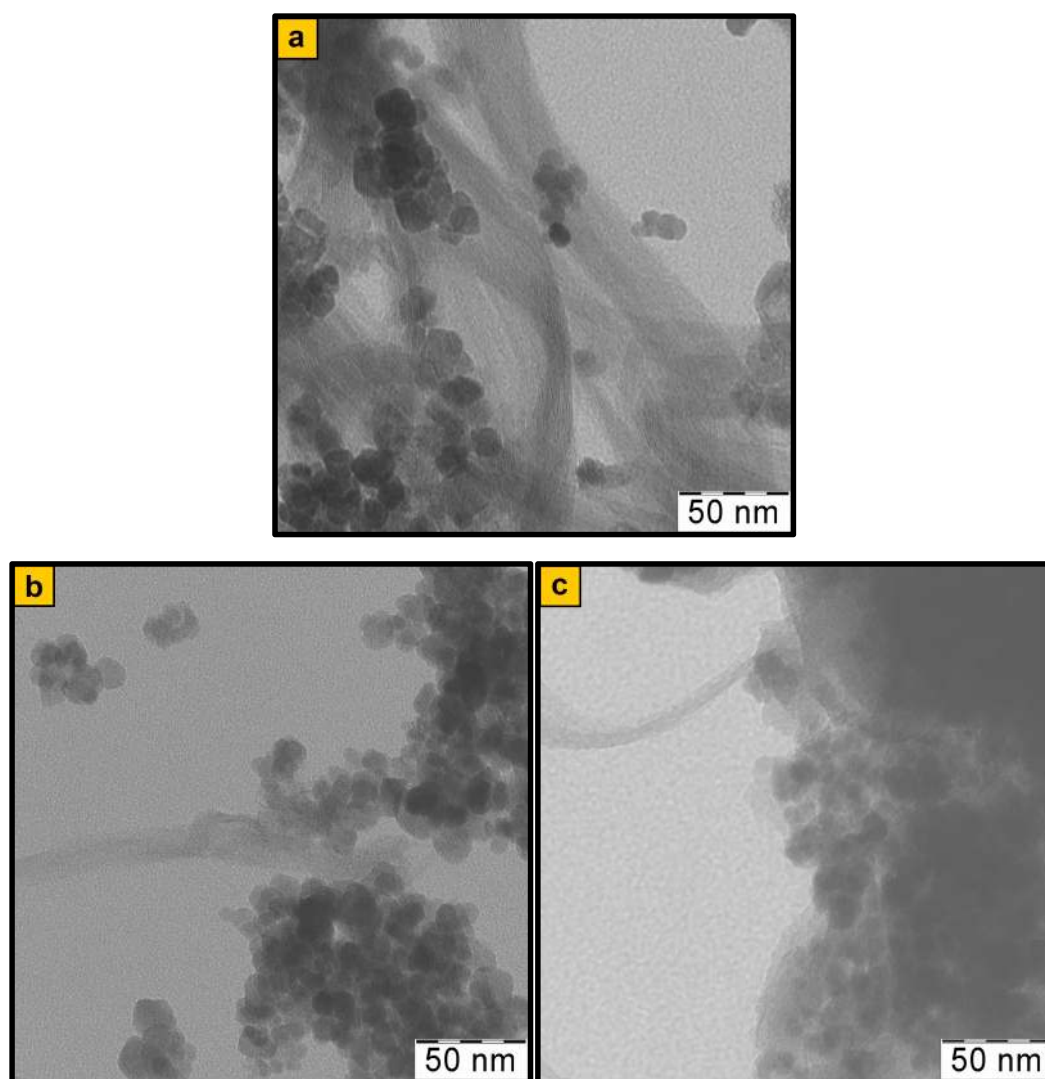
Figure 4. TEM images of Fe$_3$O$_4$/SWCNT (**a**) and Fe$_3$O$_4$/SWCNT/PDPAC, prepared in alkaline (**b**) and acidic media (**c**).
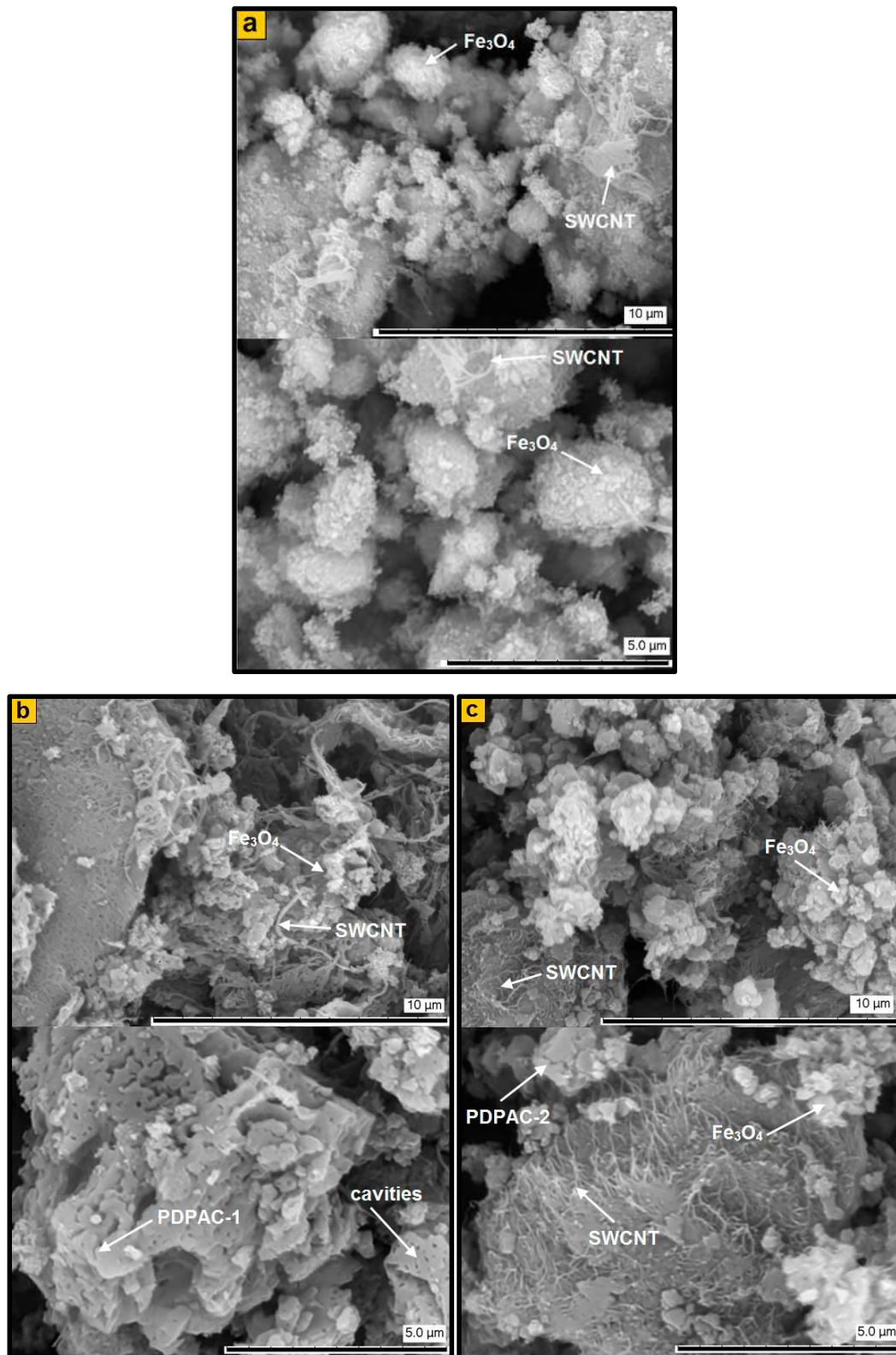
Figure 5. SEM images of Fe_3O_4/SWCNT (**a**) and Fe_3O_4/SWCNT/PDPAC, prepared in alkaline (**b**) and acidic media (**c**).
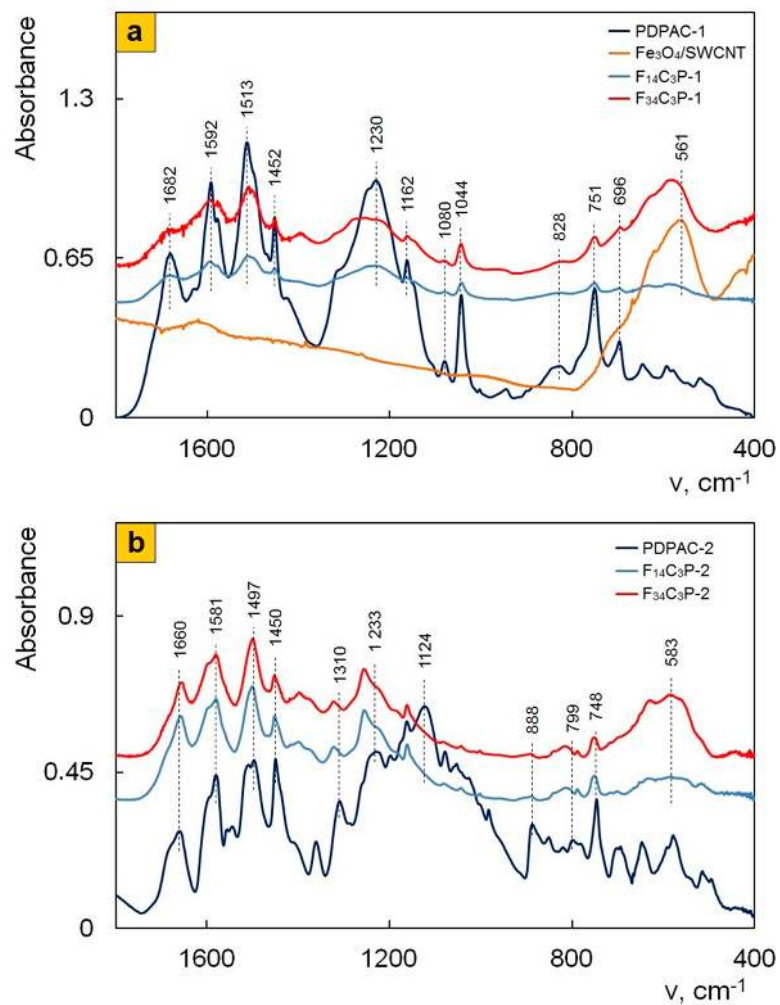
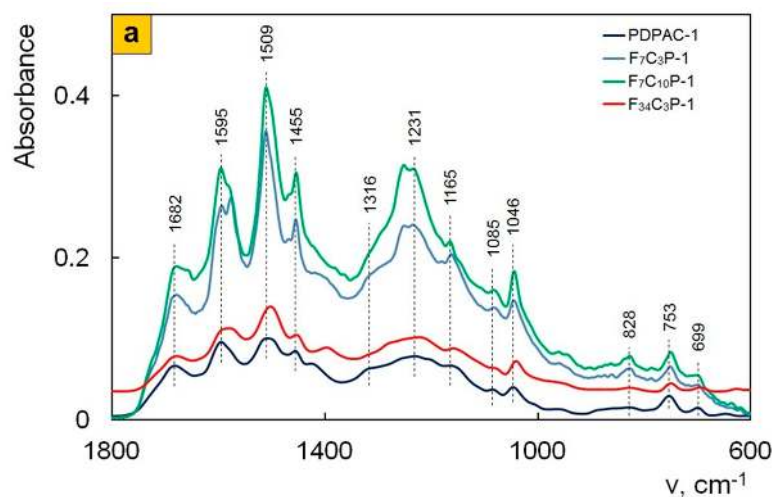**Figure 6.** FTIR spectra of PDPAC, Fe₃O₄/SWCNT, and Fe₃O₄/SWCNT/PDPAC, prepared in alkaline (**a**) and acidic media (**b**).
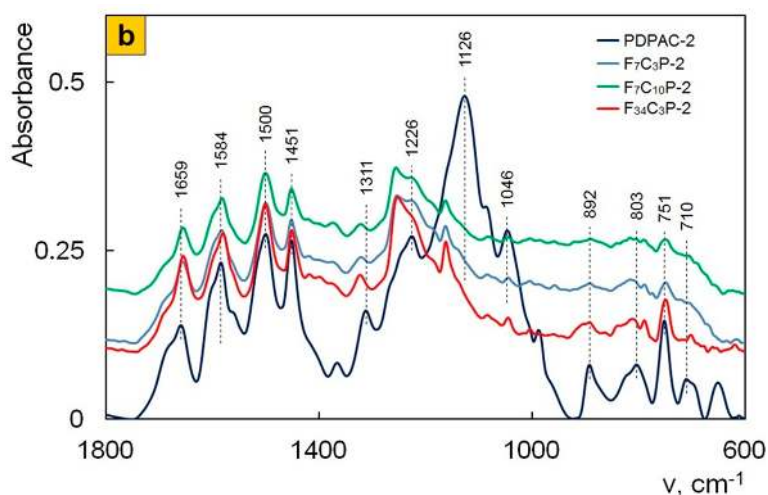

Figure 7. *Cont.*

Figure 7. Attenuated total reflection (ATR) FTIR spectra of PDPAC and Fe_3O_4/SWCNT/PDPAC, prepared in alkaline (**a**) and acidic media (**b**).

It is shown that the size and shape of Fe_3O_4 nanoparticles do not depend on the pH of the synthesis reaction medium as well. Spherical Fe_3O_4 nanoparticles are clearly visible in TEM and SEM images of the Fe_3O_4/SWCNT/PDPAC nanocomposites (Figures 4 and 5). However, the presence of an organic solvent (chloroform) in an alkaline medium leads to the formation of a polymer morphology with distinct cavities (Figure 5b). These cavities appear in places of chloroform droplets during the precipitation of the Fe_3O_4/SWCNT/PDPAC-1 nanocomposites in a sulfuric acid solution. According to the TEM data, the size of Fe_3O_4 nanoparticles in the nanomaterials is within the range of $2 < d < 14$ nm irrespective of the obtaining method (Figure 4). The size distribution of coherent scattering regions in the Fe_3O_4 nanoparticles was calculated using the XRD data (Figure 8). In the Fe_3O_4/SWCNT/PDPAC nanocomposites, about 80–90% of Fe_3O_4 crystallites are up to 5 nm in size. According to the ICP-AES, depending on the synthesis conditions, the content of iron is $C_{Fe} = 6.2$–34.7%. In the obtained ternary hybrid nanomaterials, the problem of agglomeration of nanocomposite components is solved by the fact that the polymer structure contains functional groups that interact both with magnetite nanoparticles and with carbon nanotubes, preventing their aggregation.
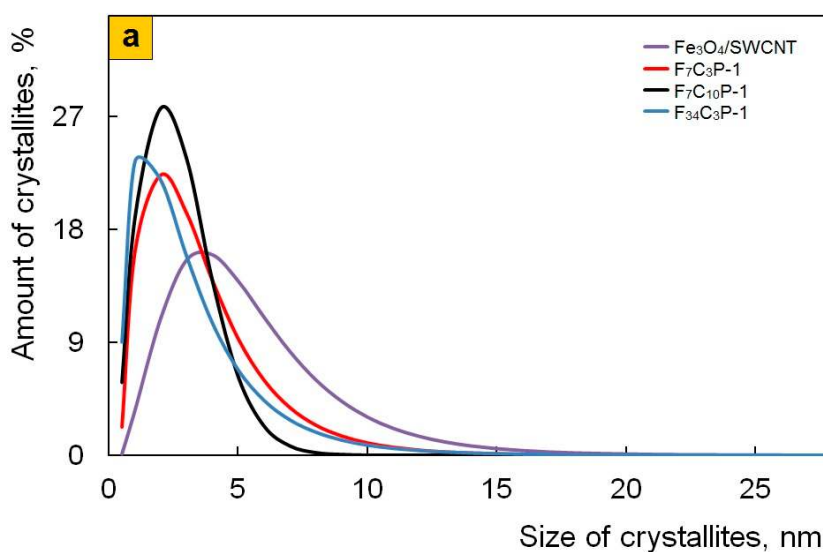

Figure 8. *Cont.*
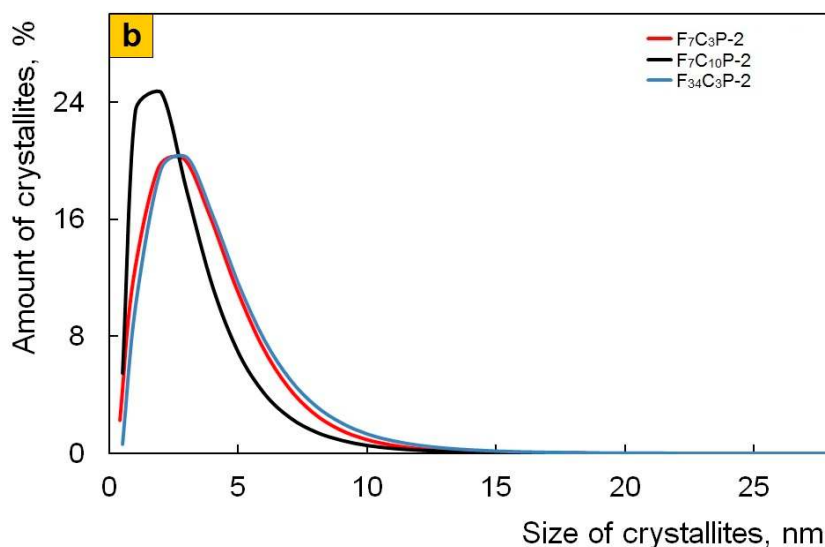
Figure 8. Fe₃O₄ crystallites size distribution in Fe₃O₄/SWCNT and Fe₃O₄/SWCNT/PDPAC, prepared in alkaline (**a**) and acidic media (**b**).

Thus, regardless of the synthesis method, the Fe₃O₄/SWCNT/PDPAC-1 and Fe₃O₄/SWCNT/PDPAC-2 nanocomposites have the same phase composition: they contain PDPAC, carbon nanotubes, and Fe₃O₄ nanoparticles. However, the Fe₃O₄/SWCNT/PDPAC-1 nanomaterials prepared in the interfacial process in an alkaline medium are metal–carbon Fe₃O₄/SWCNT nanocomposites coated with PDPAC-1, whereas the Fe₃O₄/SWCNT/PDPAC-2 nanocomposites obtained in an acidic medium are SWCNT dispersed in a polymer matrix with Fe₃O₄ nanoparticles immobilized on the SWCNT/PDPAC-2 surface (Figures 4 and 5).

Comparison of FTIR spectra of polymers and nanocomposites prepared under the same conditions (Figures 6 and 7) shows that all the main bands characterizing the chemical structure of PDPAC are retained in the FTIR spectra of Fe₃O₄/SWCNT/PDPAC regardless of the obtaining method. As can be seen in Figures 6 and 7, the chemical structure of the polymer component depends strongly on the pH of the synthesis reaction medium. It was established that during the synthesis of Fe₃O₄/SWCNT/PDPAC-1 nanocomposites in an alkaline medium (pH 11.4), the polymer chain grows via the C–C bonding of phenyl rings in 2- and 4-positions in relation to nitrogen (δ_{C-H} = 828 and 753 cm^{-1}). This differs significantly from the type of C–C bonding that takes place during the synthesis of Fe₃O₄/SWCNT/PDPAC-2 nanocomposites in an acidic medium (pH 0.3), when the polymer chain grows via the C–C bonding of phenyl rings in the *para* position relative to nitrogen (δ_{C-H} = 892 and 803 cm^{-1}). The chemical structure of the corresponding polymer components is shown in Figure 1. This dependence of the polymer matrix chemical structure on the reaction medium pH was observed during the synthesis of SWCNT/PDPAC nanocomposites in the absence of Fe₃O₄ nanoparticles [52].

As the content of carbon nanotubes increases, ATR FTIR spectra of Fe₃O₄/SWCNT/PDPAC-1 nanocomposites (Figure 7a) demonstrate a bathochromic shift in the PDPAC-1 skeletal vibration frequencies at 10–16 cm^{-1}, which indicates the π–π^* interaction of aromatic units of the polymer with the Fe₃O₄/SWCNT surface in an alkaline medium (stacking effect). The polymer formation on the Fe₃O₄/CNT surface provides the charge transfer, which is manifested in the shift of skeletal oscillation frequencies of the polymer [53–55].

As the content of carbon nanotubes grows, the FTIR spectra of Fe₃O₄/SWCNT/PDPAC-2 nanocomposites show the shift of absorption bands at 1659 and 1226 cm^{-1}, associated with stretching vibrations of $\nu_{C=O}$ in COOH groups, as well as the shift of the band at 561 to 583 cm^{-1}, corresponding to stretching vibrations of the ν_{Fe-O} bond (Figures 6 and 7). This indicates the interaction of carboxyl groups of SWCNT/PDPAC-2 with Fe₃O₄.

3.2. Electrical Characterization of Nanomaterials

Frequency dependence on the AC conductivity of Fe_3O_4/SWCNT/PDPAC nanocomposites was studied in the frequency range of 0.1 Hz–1.0 MHz (Figure 9). According to [56–58], the frequency dependence on the conductivity (σ_{ac}) is described by evaluation:

$$\sigma_{ac} = \sigma_{dc} + A\omega^n,$$

where $\omega = 2\pi f$ is the angular frequency,

σ_{dc}—the frequency independent (dc) part of conductivity,
n—the exponential parameter ($0 \le n \le 1$),
A—the thermally activated quantity.
A and n depend on the temperature and the volume fraction of the conducting component.
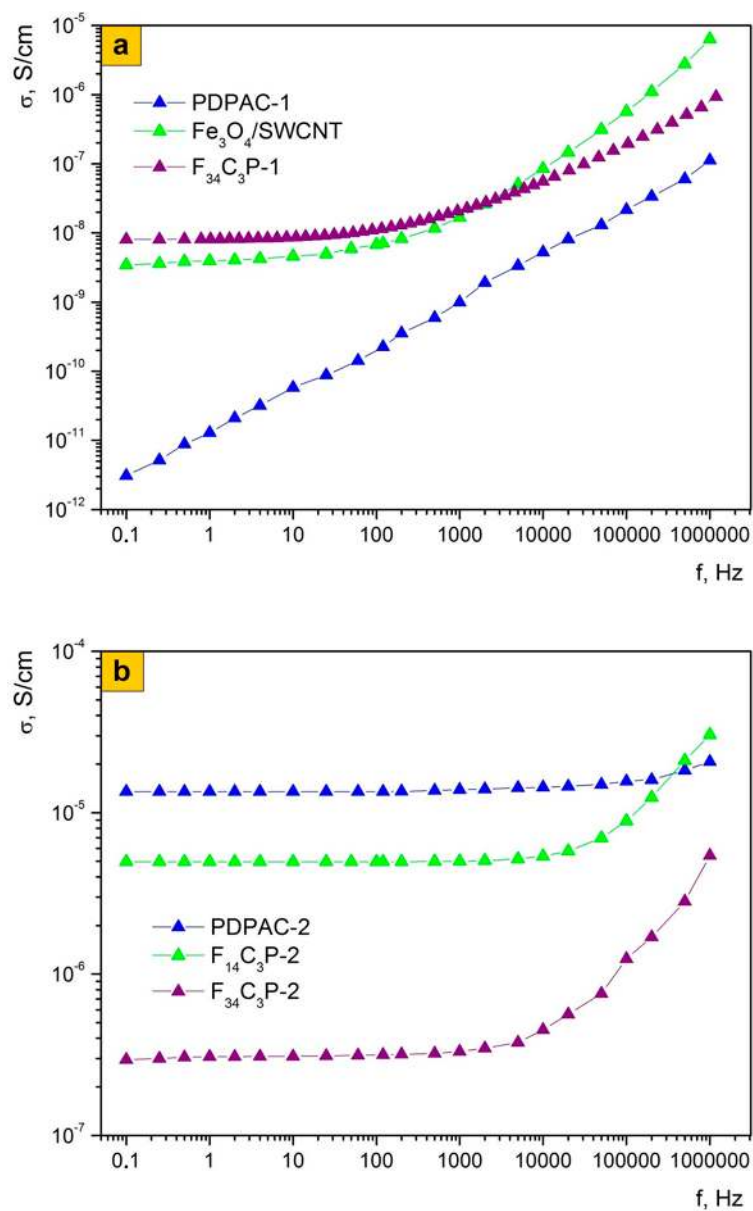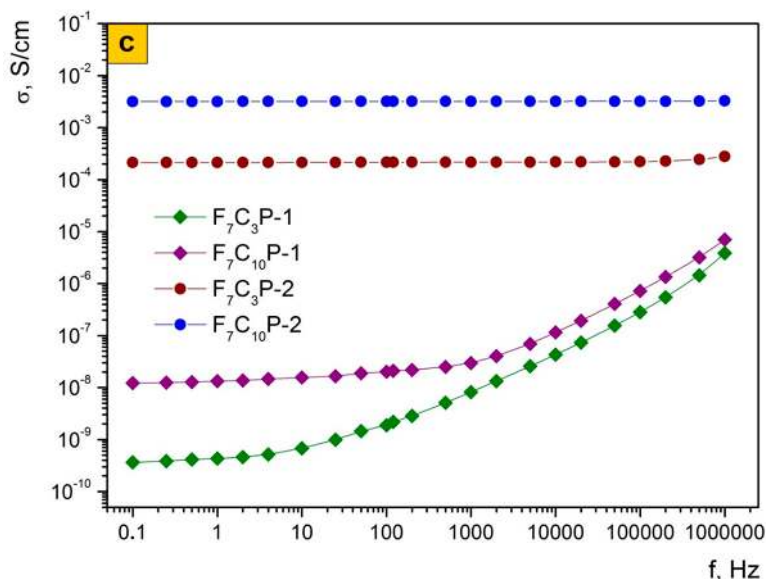

Figure 9. *Cont.*

Figure 9. Frequency dependence of the conductivity for PDPAC, Fe$_3$O$_4$/SWCNT, and Fe$_3$O$_4$/SWCNT/PDPAC, prepared in alkaline (**a**,**c**) and acidic media (**b**,**c**).

Table 3 lists the conductivity values of materials. It can be seen that the conductivity (σ_{ac}) of nanocomposites depends on the pH of the synthesis reaction medium.

Table 3. The conductivity values of materials.

Materials	* σ_{ac}, S/cm		σ_{dc}, S/cm	n	A
PDPAC-1	3.1×10^{-12}	1.1×10^{-7}	2.8×10^{-12}	0.75	8.5×10^{-12}
F$_7$C$_3$P-1	3.6×10^{-10}	1.2×10^{-7}	2.4×10^{-10}	0.82	1.7×10^{-13}
F$_7$C$_{10}$P-1	1.2×10^{-8}	9.6×10^{-7}	1.1×10^{-8}	0.96	1.9×10^{-12}
F$_{34}$C$_3$P-1	8.1×10^{-9}	8.7×10^{-7}	6.8×10^{-9}	0.99	5.4×10^{-13}
F$_{34}$C$_3$ **	3.5×10^{-9}	2.5×10^{-6}	2.3×10^{-9}	1.00	9.7×10^{-13}
PDPAC-2	1.4×10^{-5}	2.2×10^{-5}	1.0×10^{-5}	0.45	6.9×10^{-9}
F$_7$C$_3$P-2	2.5×10^{-4}	2.7×10^{-4}	2.1×10^{-4}	0.31	3.0×10^{-7}
F$_7$C$_{10}$P-2	3.7×10^{-3}	3.3×10^{-3}	3.2×10^{-3}	0.51	2.0×10^{-8}
F$_{14}$C$_3$P-2	4.6×10^{-6}	3.1×10^{-5}	4.3×10^{-6}	0.64	9.0×10^{-11}
F$_{34}$C$_3$P-2	3.4×10^{-7}	3.6×10^{-6}	3.1×10^{-7}	0.74	1.3×10^{-9}

* σ—The AC conductivity at 0.1 Hz and 1.0 MHz. ** Fe$_3$O$_4$/SWCNT.

At low frequencies, the Fe$_3$O$_4$/SWCNT/PDPAC-1 nanocomposites as well as Fe$_3$O$_4$/SWCNT are characterized by weak frequency dependence on electrical conductivity. At the same time, the electrical conductivity of nanocomposites is several orders of magnitude higher than that of PDPAC-1 (3.1×10^{-12} S/cm) and amounts to 3.5×10^{-9} S/cm (F$_{34}$C$_3$) and 8.1×10^{-9} S/cm (F$_{34}$C$_3$P-1) at 0.1 Hz (Figure 9a). Apparently, the conductivity of Fe$_3$O$_4$/SWCNT/PDPAC-1 is contributed significantly by the metal–carbon Fe$_3$O$_4$/SWCNT nanocomposite, i.e., the increase in electrical conductivity of nanomaterials is due to the presence both of SWCNT and magnetite nanoparticles. As frequency grows, the electrical conductivity of F$_{34}$C$_3$P-1 increases gradually by two orders of magnitude to 8.7×10^{-7} S/cm.

The electrical conductivity of Fe$_3$O$_4$/SWCNT/PDPAC-2 nanocomposites at low frequencies is significantly higher than the conductivity of Fe$_3$O$_4$/SWCNT/PDPAC-1. This is due to the doping of the polymer matrix that occurs during the synthesis of nanocomposites in an acidic medium. As can be seen in Figure 9b, the electrical conductivity of neat PDPAC-2 does not depend much on

frequency and amounts to $(1.4–2.2) \times 10^{-5}$ S/cm. The F_7C_3P-2 nanocomposite with a low magnetite content demonstrates an increase in its conductivity by an order of magnitude compared to PDPAC-2 up to 2.1×10^{-4} S/cm. Conductivity of carbon nanotubes contributes to the growth in electrical conductivity as well. This also explains the fact that conductivity (σ_{ac}) does not depend on frequency at low magnetite content. However, with the increase of Fe_3O_4 content in the $F_{14}C_3P$-2 and $F_{34}C_3P$-2 nanocomposites, the electrical conductivity drops to 4.6×10^{-6} S/cm and 3.1×10^{-7} S/cm, respectively. An important role in reducing the conductivity of nanocomposites belongs to the electrical conductivity of Fe_3O_4 that has a significantly lower conductivity ($\sim 10^{-10}$ S/cm) compared to the doped polymer and CNT. At the same time, the frequency dependence on the electrical conductivity is observed. As frequency increases, the electrical conductivity of $F_{14}C_3P$-2 and $F_{34}C_3P$-2 rises to 3.1×10^{-5} S/cm and 3.6×10^{-6} S/cm, respectively.

As can be seen in Figure 9c, the electrical conductivity of the nanocomposites depends on carbon nanotubes concentration. With the growth in SWCNT content from 3 to 10 wt. %, the electrical conductivity of Fe_3O_4/SWCNT/PDPAC-1 increases by two orders of magnitude from 3.6×10^{-10} S/cm (F_7C_3P-1) to 1.2×10^{-8} S/cm ($F_7C_{10}P$-1). At high frequencies, the electrical conductivity of Fe_3O_4/SWCNT/PDPAC-1 nanocomposites reaches $(1.2–9.6) \times 10^{-7}$ S/cm, depending on the content of SWCNT. With the increase in SWCNT content from 3 to 10 wt. %, the conductivity of Fe_3O_4/SWCNT/PDPAC-2 rises from 2.1×10^{-4} S/cm (F_7C_3P-2) to 3.2×10^{-3} S/cm ($F_7C_{10}P$-2). The main contribution to the growth of electrical conductivity is made by carbon nanotubes, which is confirmed by the independence of the σ_{ac} conductivity on frequency when Fe_3O_4 content is low.

Thus, as can be seen in Table 3, for all nanocomposites, the exponential parameter *n* lies in the range of $0 \leq n \leq 1$, which is typical for disperse systems with a hopping mechanism of charge transfer [43,56–60]. Since the frequency dependence on the AC conductivity of nanocomposites shows an increase with the growth in current frequency, it can be argued that the effect of tunneling is minimal. At low frequencies, the DC conductivity plays an important role, the growth of which leads to a high frequency shift of the region of sharp increase in electrical conductivity.

3.3. Thermal Properties of Nanomaterials

TGA and DSC methods were used to study thermal stability of the nanocomposites depending on the preparation process. Figure 10 shows TGA thermograms of Fe_3O_4/SWCNT/PDPAC compared to PDPAC at heating up to 1000 °C in argon flow and in air. Table 4 presents the main thermal properties of the materials. As can be seen, the weight loss curves of the obtained materials have a stepwise pattern. Weight loss at low temperatures is associated with moisture removal, which is also confirmed by the DSC data. Figure 11 shows DSC thermograms of Fe_3O_4/SWCNT/PDPAC. There is an endothermic peak at ~ 105 °C on the DSC thermograms of nanocomposites. A small endothermic peak at ~ 273 °C in the Fe_3O_4/SWCNT/PDPAC-2 is associated with the decomposition of low molecular weight oligomers. When re-heated, this peak is absent. X-ray diffraction data also confirm the content of the crystalline low molecular weight fraction (0.75–2.35%) in the nanocomposites obtained in an acidic medium (Figure 2c, Table 2).

Table 4. Thermal properties of materials.

Materials	* $T_{5\%}$, °C	** $T_{25\%}$, °C	*** $T_{50\%}$, °C	**** Residue, %
PDPAC-1	182/205	400/324	522/663	0/19
PDPAC-2	104/102	232/243	517/396	0/35
$F_{34}C_3P$-1	238/201	403/628	> 1000/910	53/48
$F_{34}C_3P$-2	180/225	388/677	542/ > 1000	48/52

* $T_{5\%}$, ** $T_{25\%}$, *** $T_{50\%}$—5, 25 and 50% weight losses (air/argon), **** residue at 1000 °C (air/argon).
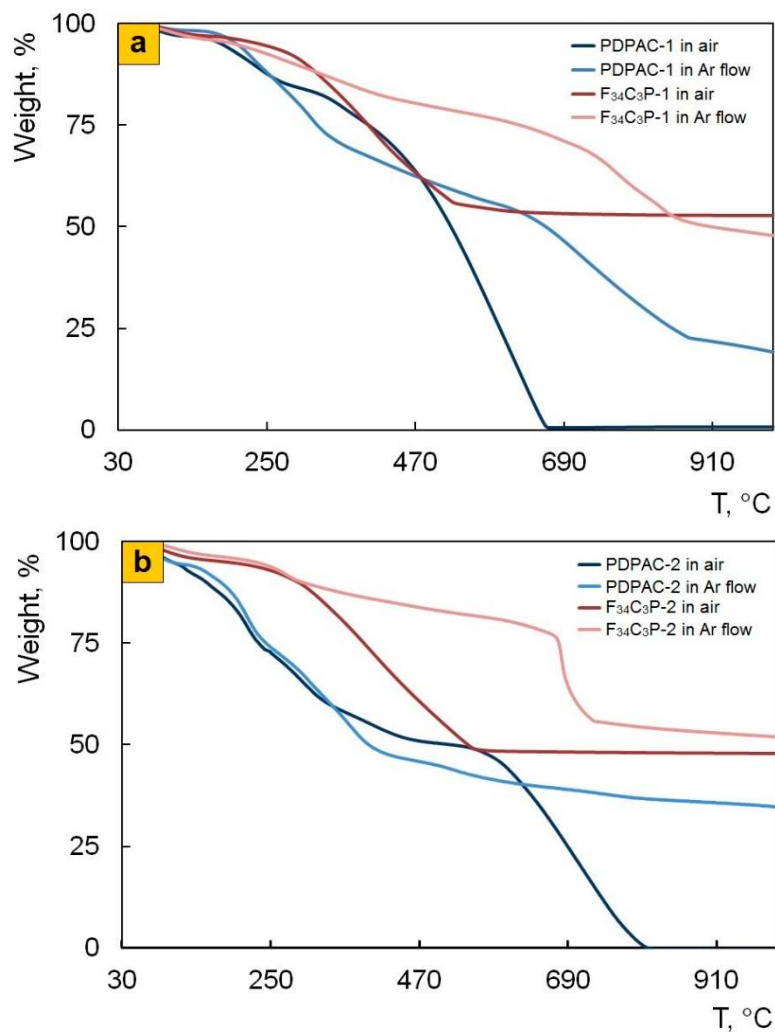
Figure 10. TGA thermograms of PDPAC and Fe_3O_4/SWCNT/PDPAC, prepared in alkaline (**a**) and acidic media (**b**), at heating up to 1000°C in the argon flow and in air.

As seen in Figure 10, both in the PDPAC-1 and PDPAC-2 polymers, the weight loss at ~170 °C is connected with the removal of COOH groups [52]. In this temperature range, the DSC thermograms of polymers have an exothermic peak associated with decomposition [44,46]. The absence of weight loss in the Fe_3O_4/SWCNT/PDPAC nanomaterials in this temperature range is explained by the fact that the carboxylate groups of the polymer interact with either the Fe_3O_4 nanoparticles or the aromatic structures of SWCNT, depending on the method of nanocomposites preparation. The DSC thermograms of nanomaterials presented in Figure 11 do not show thermal effects in this temperature range.

The resulting nanomaterials are characterized by high thermal stability that exceeds the thermal stability of PDPAC significantly. Regardless of the preparation method, the Fe_3O_4/SWCNT/PDPAC nanocomposites lose half of their initial weight in an inert atmosphere at temperatures above 900 °C. At 1000 °C, both in an inert atmosphere and in air, the residue is ~50% (Table 4).
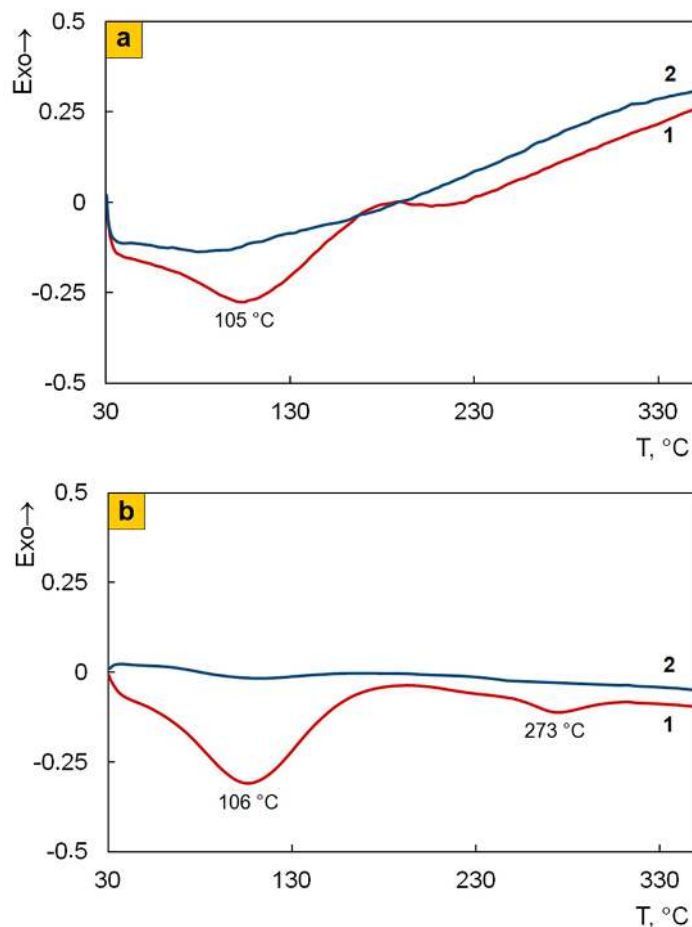
Figure 11. DSC thermograms of Fe$_3$O$_4$/SWCNT/PDPAC, prepared in alkaline (**a**) and acidic media (**b**), at heating in the nitrogen flow to 350°C (*1*—first heating, *2*—second heating).

3.4. Magnetic Properties of Nanomaterials

Magnetic properties of Fe$_3$O$_4$/SWCNT/PDPAC nanomaterials were studied and the values of their main magnetic parameters were measured. The dependence of the magnetization on the magnitude of the applied magnetic field at room temperature is shown in Figure 12. Table 5 lists the values of the main magnetic properties of nanocomposites.

Table 5. Magnetic properties of nanomaterials.

Nanomaterials	Fe, % *	H_C, Oe	M_S, emu/g	M_R, emu/g	M_R/M_S
F$_7$C$_3$P-1	6.4	0	4.8	0	0
F$_{10}$C$_3$P-1	8.4	0	11.3	0	0
F$_{14}$C$_3$P-1	12.0	0	15.7	0	0
F$_{18}$C$_3$P-1	17.9	0	22.5	0	0
F$_{34}$C$_3$P-1	33.5	0	31.6	0	0
F$_{34}$C$_3$ **	61.2	6	47.3	0.45	0.009
F$_7$C$_3$P-2	7.6	0	5.3	0	0
F$_7$C$_{10}$P-2	6.2	0	4.5	0	0
F$_{14}$C$_3$P-2	13.4	0	12.1	0	0
F$_{18}$C$_3$P-2	17.8	0	26.1	0	0
F$_{34}$C$_3$P-2	34.7	0	39.4	0	0

* According to ICP-AES data, ** Fe$_3$O$_4$/SWCNT. H_C—coercive force, M_S—saturation magnetization, M_R—residual magnetization.
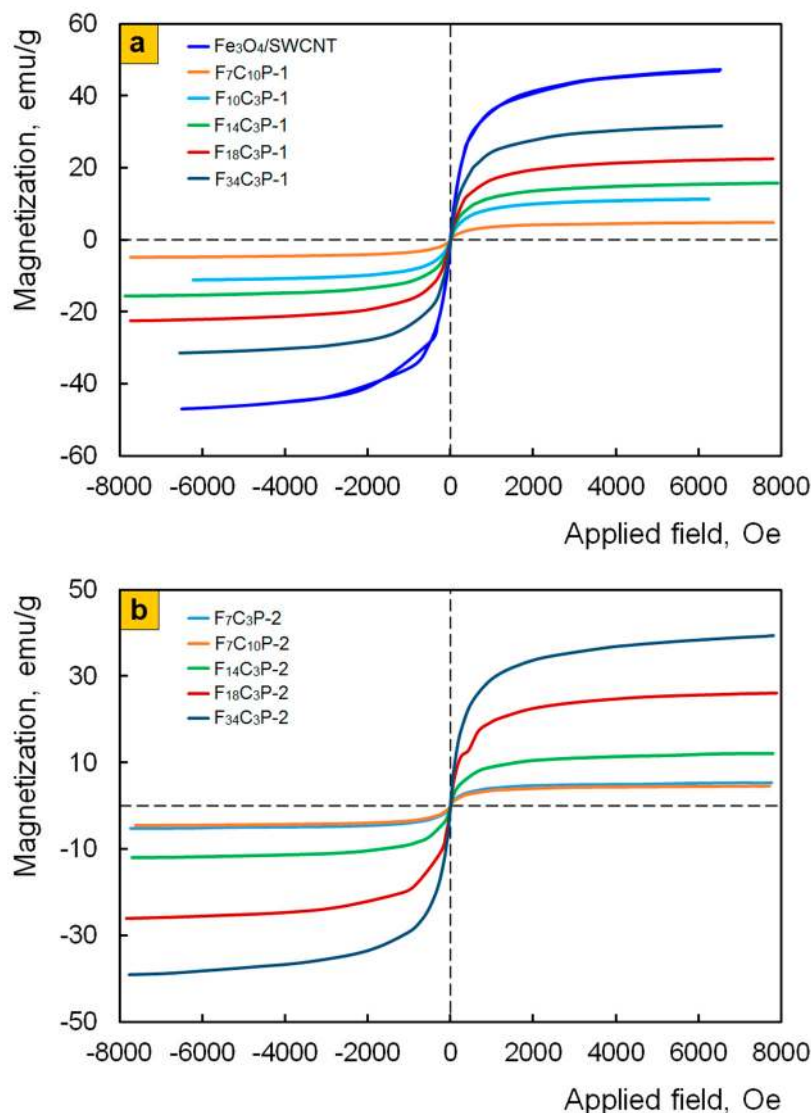
Figure 12. Magnetization of Fe$_3$O$_4$/SWCNT and Fe$_3$O$_4$/SWCNT/PDPAC, prepared in alkaline (**a**) and acidic media (**b**), as a function of applied magnetic field at room temperature.

It can be seen that, regardless of the preparation method, the Fe$_3$O$_4$/SWCNT/PDPAC nanocomposites are superparamagnetic; this is due to the small size and high dispersion of magnetic nanoparticles [49,61]. The squareness ratio of the hysteresis loop is $\kappa_S = M_R/M_S = 0$. The saturation magnetization M_S depends on the content of magnetite nanoparticles and reaches 31.6–39.4 emu/g depending on the synthesis method of nanocomposites. An increase in the concentration of SWCNT to 10 wt. % has little effect on the main magnetic parameters of the nanomaterials (Figure 12b).

The obtained hybrid nanomaterials can be promising as active components of magnetic fluids that are stable suspensions of magnetic nanoparticles in water or an organic solvent. Suspensions based on magnetic nanocomposites in ethanol were prepared. It was found that suspensions of Fe$_3$O$_4$/SWCNT/PDPAC-1 in ethanol remain stable for more than 8 months, whereas the Fe$_3$O$_4$/SWCNT/PDPAC-2 nanocomposites as well as Fe$_3$O$_4$/SWCNT dispersed in ethanol start sedimenting from the first minutes (Figure 13).

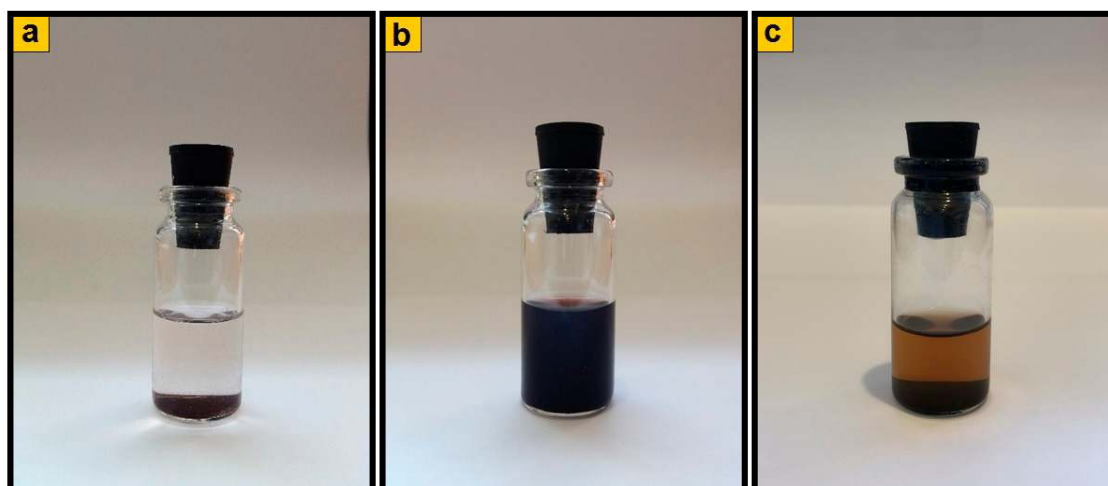**Figure 13.** Suspensions of Fe_3O_4/SWCNT (**a**) and Fe_3O_4/SWCNT/PDPAC, prepared in alkaline (**b**) and acidic media (**c**) in ethanol. (**a,c**)—in 5 min, (**b**)—in 8 months.

This behavior of the Fe_3O_4/SWCNT/PDPAC-1 and Fe_3O_4/SWCNT/PDPAC-2 nanocomposites is associated with the different chemical structures of the polymer component. The stability of the Fe_3O_4/SWCNT/PDPAC-1 suspension in ethanol is explained by the presence of a positive charge in the polymer shell structure of nanocomposites, which prevents the aggregation of magnetic nanoparticles. A positive charge can be formed both due to the charge transfer during the π-π^* interaction of aromatic polymer units with the surface of Fe_3O_4/SWCNT, and due to the electronic interaction of delocalized π-electrons with the free d-orbitals of an iron atom.

4. Conclusions

Ternary nanomaterials based on polydiphenylamine-2-carboxylic acid (PDPAC), single-walled carbon nanotubes (SWCNT), and magnetite nanoparticles in an acidic medium and in the interfacial process in an alkaline medium were obtained for the first time. The influence of the reaction medium pH on the structure, morphology, phase composition, thermal, electrical and magnetic properties of the obtained hybrid nanocomposites was studied. It was shown that the phase composition of Fe_3O_4/SWCNT/PDPAC as well as the size and shape of Fe_3O_4 nanoparticles do not depend on the reaction medium pH. The size of spherical Fe_3O_4 nanoparticles is within the range of $2 < d < 14$ nm. Regardless of the preparation method, the nanomaterials are superparamagnetic ($\kappa_S = M_R/M_S = 0$). The Fe_3O_4/SWCNT/PDPAC nanomaterials lose half of their initial weight in an inert atmosphere at temperatures above 900 °C. Electrical conductivity of the nanomaterials depends strongly on the synthesis method as well as on the concentration both of carbon nanotubes and of Fe_3O_4 nanoparticles. At the same time, at low frequencies, the electrical conductivity of Fe_3O_4/SWCNT/PDPAC-2 nanocomposites is significantly higher than the conductivity of Fe_3O_4/SWCNT/PDPAC-1 due to the polymer matrix doping in an acidic medium. It was shown that, unlike Fe_3O_4/SWCNT/PDPAC-2, the Fe_3O_4/SWCNT/PDPAC-1 nanomaterials prepared in an alkaline medium form magnetic fluids in ethanol; this is connected with differences in the chemical structure of the polymer component. Therefore, the results indicate that prepared hybrid electromagnetic nanomaterials have potential applications in the manufacture of sensors, supercapacitors, rechargeable batteries, anti-corrosion coatings, materials absorbing electromagnetic radiation, etc. The ability of powders of the prepared ternary hybrid nanocomposites to form suspensions in water and organic media allows to obtain the nanocomposite-based coatings on smooth and rough surfaces. Furthermore, these ternary nanocomposite-based suspensions can be applied for the impregnation of porous supports. These processing methods are important at fabrication of electrodes for chemical current sources and energy storage, electromagnetic shielding, sensor sensitive elements, anti-corrosion protection, etc.

References

1. Sellinger, A.; Weiss, P.M.; Nguyen, A.; Lu, Y.; Assink, R.A.; Gong, W.; Brinker, C.J. Continuous self-assembly of organic–inorganic nanocomposite coatings that mimic nacre. *Nature* **1998**, *394*, 256–259. [CrossRef]

2. Yamamoto, K.; Sakata, Y.; Nohara, Y.; Takashi, Y.; Tatsumi, T. Organic-inorganic hybrid zeolites containing organic frameworks. *Science* **2003**, *300*, 470–472. [CrossRef]

3. Balazs, A.C.; Emrick, T.; Russel, T.P. Nanoparticle polymer composites: Where two small worlds meet. *Science* **2006**, *314*, 1107–1110. [CrossRef]

4. Karpacheva, G.P. Hybrid magnetic nanocomposites including polyconjugated polymers. *Polym. Sci. C* **2016**, *58*, 131–146.

5. Zheng, Y.; Wang, X.; Wu, G. Chemical modification of carbon fiber with diethylenetriaminepentaacetic acid/halloysite nanotube as a multifunctional interfacial reinforcement for silicone resin composites. *Polym. Adv. Technol.* **2020**, *31*, 527–535. [CrossRef]

6. Zheng, Y.; Chen, L.; Wang, X.; Wu, G. Modification of renewable cardanol onto carbon fiber for the improved interfacial properties of advanced polymer composites. *Polymers* **2020**, *12*, 45. [CrossRef]

7. Godovsky, D.Y. Device applications of polymer-nanocomposites. *Adv. Polym. Sci.* **2000**, *153*, 163–205.

8. Gerasin, V.A.; Antipov, E.M.; Karbushev, V.V.; Kulichikhin, V.G.; Karpacheva, G.P.; Talroze, R.V.; Kudryavtsev, Y.V. New approaches to the development of hybrid nanocomposites: From structural materials to high-tech applications. *Russ. Chem. Rev.* **2013**, *82*, 303–332. [CrossRef]

9. Yang, J.; Liu, Y.; Liu, S.; Li, L.; Zhang, C.; Liu, T. Conducting polymer composites: Material synthesis and applications in electrochemical capacitive energy storage. *Mater. Chem. Front.* **2017**, *1*, 251–268. [CrossRef]

10. Lyu, L.; Liu, J.; Liu, H.; Liu, C.; Lu, Y.; Sun, K.; Fan, R.; Wang, N.; Guo, Z.; Wujcik, E.K. An overview of electrically conductive polymer nanocomposites toward electromagnetic interference shielding. *Eng. Sci.* **2018**, *2*, 26–42.

11. Zhao, B.; Deng, J.; Zhang, R.; Liang, L.; Fan, B.; Bai, Z.; Shao, G.; Park, C.B. Recent advances on the electromagnetic wave absorption properties of Ni based materials. *Eng. Sci.* **2018**, *3*, 5–40. [CrossRef]

12. He, Y.; Chen, Q.; Yang, S.; Lu, C.; Feng, M.; Jiang, Y.; Cao, G.; Zhang, J.; Liu, C. Micro-crack behavior of carbon fiber reinforced Fe$_3$O$_4$/graphene oxide modified epoxy composites for cryogenic application. *Compos. Part A Appl. Sci. Manuf.* **2018**, *108*, 12–22. [CrossRef]

13. Wang, C.; Murugadoss, V.; Kong, J.; He, Z.; Mai, X.; Shao, Q.; Chen, Y.; Guo, L.; Liu, C.; Angaiah, S.; et al. Overview of carbon nanostructures and nanocomposites for electromagnetic wave shielding. *Carbon* **2018**, *140*, 696–733. [CrossRef]

14. Chen, J.; Yu, Q.; Cui, X.; Dong, M.; Zhang, J.; Wang, C.; Fan, J.; Zhu, Y.; Guo, Z. An overview of stretchable strain sensors from conductive polymer nanocomposites. *J. Mater. Chem. C* **2019**, *7*, 11710–11730. [CrossRef]

15. Wen, N.; Jiang, B.; Wang, X.; Shang, Z.; Jiang, D.; Zhang, L.; Sun, C.; Wu, Z.; Yan, H.; Liu, C.; et al. Overview of polyvinyl alcohol nanocomposite hydrogels for electro-skin, actuator, supercapacitor and fuel cell. *Chem. Rec.* **2020**. [CrossRef]

16. Wei, H.; Wang, H.; Cui, D.; Zhao, Z.; Chu, L.; Wei, X.; Wang, L.; Pan, D.; Fan, J.; Li, Y.; et al. Multifunctions of polymer nanocomposites: Environmental remediation, electromagnetic interference shielding, and sensing applications. *ChemNanoMat* **2020**, *6*, 174–184. [CrossRef]

17. Zhang, L.; Du, W.Y.; Nautiyal, A.; Liu, Z.; Zhang, X.Y. Recent progress on nanostructured conducting polymers and composites: Synthesis, application and future aspects. *Sci. China Mater.* **2018**, *61*, 303–352. [CrossRef]

18. Jiang, D.W.; Murugadoss, V.; Wang, Y.; Lin, J.; Ding, T.; Wang, Z.C.; Shao, Q.; Wang, C.; Liu, H.; Lu, N. Electromagnetic interference shielding polymers and nanocomposites—A Review. *Polym. Rev.* **2019**, *59*, 280–337. [CrossRef]

19. Zhang, Y.J.; Lin, Y.W.; Chang, C.C.; Wu, T.M. Conducting and magnetic behaviors of polyaniline coated multi-walled carbon nanotube composites containing monodispersed magnetite nanoparticles. *Synth. Met.* **2011**, *161*, 937–942. [CrossRef]

20. Chen, T.; Qiu, J.; Zhu, K.; Che, Y.; Zhang, Y.; Zhang, J.; Li, H.; Wang, F.; Wang, Z. Enhanced electromagnetic wave absorption properties of polyaniline-coated Fe_3O_4/reduced graphene oxide nanocomposites. *J. Mater. Sci. Mater. Electron.* **2014**, *25*, 3664–3673. [CrossRef]

21. Zhou, H.; Wang, X.; Yu, K.; Zhang, C.; Li, H.; Du, Z. Preparation of multi-walled carbon nanotube/polyaniline/Fe_3O_4 composites. *Integr. Ferroelectr.* **2014**, *154*, 159–165. [CrossRef]

22. Liu, P.; Huang, Y.; Zhang, X. Superparamagnetic Fe_3O_4 nanoparticles on graphene–polyaniline: Synthesis, characterization and their excellent electromagnetic absorption properties. *J. Alloys Compd.* **2014**, *596*, 25–31. [CrossRef]

23. Wu, T.M.; Yen, S.J.; Chen, E.C.; Chiang, R.K. Synthesis, characterization, and properties of monodispersed magnetite coated multi-walled carbon nanotube/polypyrrole nanocomposites synthesized by *in-situ* chemical oxidative polymerization. *J. Polym. Sci. B Polym. Phys.* **2008**, *46*, 727–733. [CrossRef]

24. He, Z.; Fang, Y.; Wang, X.; Pang, H. Microwave absorption properties of PANI/CIP/Fe_3O_4 composites. *Synth. Met.* **2011**, *161*, 420–425. [CrossRef]

25. Liu, P.; Huang, Y.; Wang, L.; Zhang, W. Preparation and excellent microwave absoption property of three component nanocompostes: Polyaniline-reduced graphene oxide—Co_3O_4 nanoparticles. *Synth. Met.* **2013**, *177*, 89–93. [CrossRef]

26. Yang, R.B.; Reddy, P.M.; Chang, C.J.; Chen, P.A.; Chen, J.K.; Chang, C.C. Synthesis and characterization of Fe_3O_4/polypyrrole/carbon nanotube composites with tunable microwave absorption properties: Role of carbon nanotube and polypyrrole content. *Chem. Eng. J.* **2016**, *285*, 497–507. [CrossRef]

27. Ma, Y.; Zhou, Y.; Sun, Y.; Chen, H.; Xiong, Z.; Li, X.; Shen, L.; Liu, Y. Tunable magnetic properties of Fe_3O_4/rGO/PANI nanocomposites for enhancing microwave absorption performance. *J. Alloys Compd.* **2019**, *796*, 120–130. [CrossRef]

28. Wang, S.; Bao, H.; Yang, P.; Chen, G. Immobilization of trypsin in polyaniline-coated nano-Fe_3O_4/carbon nanotube composite for protein digestion. *Anal. Chim. Acta* **2008**, *612*, 182–189. [CrossRef]

29. Radhakrishnan, S.; Krishnamoorthy, K.; Sekar, C.; Wilson, J.; Kim, S.J. A promising sensing platform on ternary composite of polyaniline-Fe_2O_3-reduced graphene oxide for sensitive hydroquinone determination. *Chem. Eng. J.* **2015**, *259*, 594–602. [CrossRef]

30. Giri, S.; Ghosh, D.; Das, C.K. In situ synthesis of cobalt doped polyaniline modified graphene composites for high performance supercapacitor electrode materials. *J. Electroanal. Chem.* **2013**, *697*, 32–45. [CrossRef]

31. Xiong, P.; Huang, H.; Wang, X. Design and synthesis of ternary cobalt ferrite/graphene/polyaniline hierarchical nanocomposites for high-perfomance supercapacitors. *J. Power Sources* **2014**, *245*, 937–946. [CrossRef]

32. Lin, H.; Huang, Q.; Wang, J.; Jiang, J.; Liu, F.; Chen, Y.; Wang, C.; Lu, D.; Han, S. Self-assembled graphene/polyaniline/Co_3O_4 ternary hybrid aerogels for supercapacitors. *Electrochim. Acta* **2016**, *191*, 444–451. [CrossRef]

33. Ren, G.; Li, Y.; Guo, Z.; Xiao, G.; Zhu, Y.; Dai, L.; Jiang, L. A bio-inspired Co_3O_4-polypyrrole-graphene complex as an efficient oxygen reduction catalyst in one-step ball milling. *Nano Res.* **2015**, *8*, 3461–3471. [CrossRef]

34. Liu, Y.; Li, J.; Li, F.; Li, W.; Yang, H.; Zhang, X.; Liu, Y.; Ma, J. A facile preparation of $CoFe_2O_4$ nanoparticles on polyaniline-functionalised carbon nanotubes as enhanced catalysts for the oxygen evolution reaction. *J. Mater. Chem. A* **2016**, *4*, 4472–4478. [CrossRef]

35. Zhao, C.; Jin, Y.; Du, X.; Du, W. In situ prepared amorphous FeCoO- polyaniline/multiwalled carbon nanotube nanohybrids as efficient oxygen evolution catalysts for rechargeable Zn-air batteries. *J. Power. Sources* **2018**, *399*, 337–342. [CrossRef]

36. Zhu, A.; Shi, P.; Sun, S.; Rui, M. Construction of rGO/Fe_3O_4/PANI nanocomposites and its corrosion resistance mechanism in waterborne acrylate-amino coating. *Prog. Org. Coat.* **2019**, *133*, 117–124. [CrossRef]

37. Singh, A.P.; Mishra, M.; Sambyal, P.; Gupta, B.K.; Singh, B.P.; Chandra, A.; Dhawan, S.K. Encapsulation of γ-Fe_2O_3 decorated reduced graphene oxide in polyaniline core–shell tubes as an exceptional tracker for electromagnetic environmental pollution. *J. Mater. Chem. A* **2014**, *2*, 3581–3593. [CrossRef]

38. Ibrahim, A.; Abdel-Aziz, M.H.; Zorombam, M.S.; Al-Hossainy, A.F. Structural, optical, and electrical properties of multi-walled carbon nanotubes/polyaniline/Fe_3O_4 ternary nanocomposites thin film. *Synth. Met.* **2018**, *238*, 1–13. [CrossRef]

39. Kong, L.; Lu, X.; Zhang, W. Facile synthesis of multifunctional multiwalled carbon nanotubes/Fe_3O_4 nanoparticles/polyaniline composite nanotubes. *J. Solid State Chem.* **2008**, *181*, 628–636. [CrossRef]

40. Cao, M.S.; Yang, J.; Song, W.L.; Zhang, D.Q.; Wen, B.; Jin, H.B.; Hou, Z.L.; Yuan, J. Ferroferric oxide/multiwalled carbon nanotube vs polyaniline/ferroferric oxide/multiwalled carbon nanotube multiheterostructures for highly effective microwave absorption. *ACS Appl. Mater. Interfaces* **2012**, *4*, 6949–6956. [CrossRef]

41. Dai, L.; Mau, A.V.H. Controlled synthesis and modification of carbon nanotubes and C_{60}: Carbon nanostructures for advanced polymeric composite materials. *Adv. Mater.* **2001**, *13*, 899–913. [CrossRef]

42. Baughman, R.H.; Zakhidov, A.A.; de Heer, W.A. Carbon nanotubes—The route toward applications. *Science* **2002**, *297*, 787–792. [CrossRef]

43. Ozkan, S.Z.; Karpacheva, G.P.; Chernavskii, P.A.; Dzidziguri, E.L.; Bondarenko, G.N.; Pankina, G.V. Hybrid materials based on poly-3-amine-7-methylamine-2-methylphenazine and magnetite nanoparticles immobilized on single-walled carbon nanotubes. *Polymers* **2018**, *10*, 544. [CrossRef] [PubMed]

44. Ozkan, S.Z.; Eremeev, I.S.; Karpacheva, G.P.; Bondarenko, G.N. Oxidative polymerization of N-phenylanthranilic acid in the heterophase system. *Open J. Polym. Chem.* **2013**, *3*, 63–69. [CrossRef]

45. Massart, R. Preparation of aqueous magnetic liquids in alkaline and acidic media. *IEEE Trans. Magn.* **1981**, *17*, 1247–1248. [CrossRef]

46. Ozkan, S.Z.; Bondarenko, G.N.; Karpacheva, G.P. Oxidative polymerization of diphenylamine-2-carboxylic acid: Synthesis, structure, and properties of polymers. *Polym. Sci. B* **2010**, *52*, 263–269. [CrossRef]

47. Ozkan, S.Z.; Eremeev, I.S.; Karpacheva, G.P.; Prudskova, T.N.; Veselova, E.V.; Bondarenko, G.N.; .Shandryuk, G.A. Polymers of dipheylamine-2-carboxylic acid: Synthesis, structure and properties. *Polym. Sci. B* **2013**, *55*, 107–115.

48. Dzidziguri, E.L. Dimensional characteristics of nanopowders. *Nanotechnologies Russ.* **2009**, *4*, 857–870. [CrossRef]

49. Chernavskii, P.A.; Pankina, G.V.; Lunin, V.V. Magnetometric methods of investigation of supported catalysts. *Russ. Chem. Rev.* **2011**, *80*, 579–604. [CrossRef]

50. Soloveva, A.Y.; Ioni, Y.V.; Gubin, S.P. Synthesis of Fe_3O_4 nanoparticles on the surface of graphene. *Mendeleev Commun.* **2016**, *26*, 38–39. [CrossRef]

51. Abrosimova, G.E.; Aronin, A.S.; Kholstinina, N.N. On the determination of the volume fraction of the crystalline phase in amorphous-crystalline alloys. *Phys. Solid State* **2010**, *52*, 445–451. [CrossRef]

52. Ozkan, S.Z.; Karpacheva, G.P.; Kostev, A.I.; Bondarenko, G.N. Formation features of hybrid nanocomposites based on polydiphenylamine-2-carboxylic acid and single-walled carbon nanotubes. *Polymers* **2019**, *11*, 1181. [CrossRef]

53. Zengin, H.; Zhou, W.; Jin, J.; Czerw, R.; Smith, D.W., Jr.; Echegoyen, L.; Carroll, D.L.; Foulger, S.H.; Ballato, J. Carbon nanotube doped polyaniline. *Adv. Mater.* **2002**, *14*, 1480–1483. [CrossRef]

54. Cochet, M.; Maser, W.K.; Benito, A.M.; Callejas, M.A.; Martínez, M.T.; Benoit, J.-M.; Schreiber, J.; Chauvet, O. Synthesis of a new polyaniline/nanotube composite: "*in-situ*" polymerisation and charge transfer through site-selective interaction. *Chem. Commun.* **2001**, *37*, 1450–1451. [CrossRef]

55. Xu, J.; Yao, P.; Liu, L.; Jiang, Z.; He, F.; Li, M.; Zou, J. Synthesis and characterization of an organic soluble and conducting polyaniline-grafted multiwalled carbon nanotube core–shell nanocomposites by emulsion polymerization. *J. Appl. Polym. Sci.* **2010**, *118*, 2582–2591. [CrossRef]

56. Jonscher, A.K. The 'universal' dielectric response. *Nature* **1977**, *267*, 673–679. [CrossRef]

57. Dyre, J.C.; Schrøder, T.B. Universality of ac conduction in disordered solids. *Rev. Mod. Phys.* **1999**, *72*, 873–892. [CrossRef]

58. Xie, P.; Li, Y.; Hou, Q.; Sui, K.; Liu, C.; Fu, X.; Zhang, J.; Murugadoss, V.; Fan, J.; Wang, Y.; et al. Tunneling-induced negative permittivity in Ni/MnO nanocomposites by a bio-gel derived strategy. *J. Mater. Chem. C.* **2020**, *8*, 3029–3039. [CrossRef]

59. Rehwald, W.; Kiess, H.; Binggeli, B. Frequency dependent conductivity in polymers and other disordered materials. *Z. Phys. B Condens. Matter.* **1987**, *68*, 143–148. [CrossRef]

60. Dyre, J.C. The random free-energy barrier model for ac conduction in disordered solids. *J. Appl. Phys.* **1988**, *64*, 2456–2468. [CrossRef]

61. Gubin, S.P.; Koksharov, Y.A.; Khomutov, G.B.; Yurkov, G.Y. Magnetic nanoparticles: Preparation, structure and properties. *Russ. Chem. Rev.* **2005**, *7*, 489–520. [CrossRef]